Optical Engineering

OpticalEngineering.SPIEDigitalLibrary.org

Performance analysis of multiple-input multiple-output free-space optical systems with partially coherent Gaussian beams and finite-sized detectors

Muhsin Caner Gökçe
Yahya Baykal
Murat Uysal

SPIE.

Muhsin Caner Gökçe, Yahya Baykal, Murat Uysal, "Performance analysis of multiple-input multiple-output free-space optical systems with partially coherent Gaussian beams and finite-sized detectors," *Opt. Eng.* **55**(11), 111607 (2016), doi: 10.1117/1.OE.55.11.111607.

Performance analysis of multiple-input multiple-output free-space optical systems with partially coherent Gaussian beams and finite-sized detectors

Muhsin Caner Gökçe,[a,*] Yahya Baykal,[b] and Murat Uysal[c]
[a]Çankaya University, Department of Electronic and Communication Engineering, Yukarıyurtçu mah. Mimar Sinan cad. Etimesgut, Ankara 06790, Turkey
[b]Çankaya University, Department of Electrical-Electronics Engineering, Yukarıyurtçu mah. Mimar Sinan cad. Etimesgut, Ankara 06790, Turkey
[c]Özyeğin University, Department of Electrical-Electronics Engineering, Nisantepe Mevki Orman sk. No: 13 Alemdağ/Çekmeköy, İstanbul 34794, Turkey

Abstract. Multiple-input multiple-output (MIMO) techniques are employed in free-space optical (FSO) links to mitigate the degrading effects of atmospheric turbulence. We consider a MIMO FSO system, which consists of a radial laser array with partially coherent Gaussian beams at the transmitter and a detector array with Gaussian apertures at the receiver. The average power and the power correlation function at the finite-sized receiver apertures are formulated by using the extended Huygens–Fresnel principle in weak atmospheric turbulence. This let us further quantify the performance metrics such as the power scintillation index, the aperture averaging factor, and the average bit error rate (BER) as functions of system parameters. The derived power scintillation equation correctly reduces to the existing coherent and partially coherent Gaussian beam scintillation indices in the limiting cases. Using the performance metrics, we analyze the effect of various practical system parameters on the performance of a MIMO FSO system. Practical system parameters include the transmitter and receiver ring radius, number of beamlets, number of finite-aperture receivers, source size, degree of source coherence, receiver aperture radius, link distance, and the structure constant of atmosphere. [DOI: 10.1117/1.OE.55.11.111607]

Keywords: multiple-input multiple-output systems; free-space optical communication; optical wave propagation; power scintillation; aperture averaging; bit error rate.

Paper 160714SS received May 8, 2016; accepted for publication Jul. 26, 2016; published online Aug. 10, 2016.

1 Introduction

Atmospheric turbulence results in the fluctuations of the received optical signal, quantified by the scintillation index. Intensity fluctuations degrade the free-space optical (FSO) link performance.[1] In order to improve the link performance, scintillation can be mitigated by aperture averaging, the use of partially coherent light sources or spatial diversity techniques that involve the use of multiple transmit and receive elements.

Aperture averaging is practically achieved by enlarging the receiver aperture with the aim of averaging patches on the optical wavefront as well as increasing the mean signal-to-noise ratio (SNR). The use of aperture averaging for reduction in scintillation has been widely investigated under the assumption of plane, spherical, and Gaussian beam wave propagations.[2–6] Aperture averaging is usually quantified by aperture averaging factor, which is defined as the ratio of power scintillation normalized by the intensity scintillation on the axis. The exact expressions for aperture averaging factor have been developed in the presence of weak atmospheric turbulence for both plane and spherical waves.[3] The effect of beam shaping on the aperture averaging factor has been further studied considering different beam shapes such as the Gaussian, flat topped, and annular beams.[4–6]

The use of partially coherent source is another method to reduce scintillation at the receiver, in spite of larger beam footprint and lower average received power. Performance analysis of partially coherent Gaussian beams in FSO links is investigated in several works.[7–12] Specifically, Fante formulated the scintillation index of incoherent beam for both slow and fast detectors.[7] A similar study is reported for partially coherent Gaussian beams.[8] Furthermore, the scintillation index of multiple and array beams with different types of partially coherent beam shapes are investigated for a point detector.[9,10] Moreover, the joint effect of aperture averaging and the use of a partially coherent source on the performance of FSO links is reported.[11] Recently, an experimental work has demonstrated that a partially coherent beam shows lower scintillation with respect to the coherent beam in any link ranges.[12]

Spatial diversity offers an alternative to conventional single-input single-output (SISO) system through the use of multiple transmitter beams and/or receiver apertures that may help to mitigate the scintillation effect of atmospheric turbulence. Scintillation reduction obtained from spatial diversity is based on the fact that since the correlation length of the received signal is of the order of centimeters in FSO links, multiple separated beams, and/or receiver apertures constitute statistically independent signal channels, which may help to provide diversity gain. In addition, transmit

*Address all correspondence to: Muhsin Caner Gökçe, E-mail: mgokce@cankaya.edu.tr

0091-3286/2016/$25.00

optical power and the received SNR are enhanced as well.[1] There are a number of different spatial diversity techniques that can be employed in FSO links. These techniques are implemented either at the transmitter (multiple-input single-output, MISO) or at the receiver (single-input multiple-output, SIMO) or at both of them (multiple-input multiple-output, MIMO).

MISO/SIMO and MIMO techniques have been widely studied in the literature by taking into consideration plane and spherical wave assumption. The closed-form expression for the outage probability in MISO FSO links are derived.[13] Performance analysis of the MISO FSO system is investigated in terms of the beam averaging factor and the average bit error rate (BER).[14] BER and outage capacity analysis of the SIMO FSO system are investigated by considering independent fading channels.[15] Furthermore, BER expressions for MIMO FSO links are derived considering both spatially independent and correlated channels.[16] Similar studies are presented in Refs. 17–20.

The performance analysis of FSO links with spatial diversity generally depends on the unbounded plane or spherical wave (point source) assumptions for mathematical simplicity. However, working with practical system parameters such as the finite source size, spacing pattern of the transmitter, receiver apertures, and the degree of source coherence is much more realistic when practical FSO systems are considered.[21] As initial attempts toward this, field correlation, aperture averaging, and BER of the MISO FSO system have been investigated by using Gaussian beam array.[22–26] To our knowledge, joint effects of the partially coherent multiple transmitter and receiver apertures on the system performance of MIMO FSO links employing finite-size receivers are not investigated.

In this paper, we consider an MIMO FSO system, which consists of a radial laser array with partially coherent Gaussian beams at the transmitter and a detector array with Gaussian apertures at the receiver. We first formulate the average power and the power correlation function at the finite-sized receiver apertures by using the extended Huygens–Fresnel principle. This let us quantify the performance metrics such as the power scintillation index, the aperture averaging factor, and the BER.

The remainder of this paper is organized as follows. In Sec. 2.1, we introduce the MIMO FSO system model under consideration. In Sec. 2.2, we calculate the total average power and the average of the square of the power on the receiver apertures. In Sec. 2.3, we analyze the performance metrics, which are the power scintillation index, the aperture averaging factor, and the average BER. In Sec. 3, we present our numerical results and finally conclude in Sec. 4.

2 System Model and Mathematical Formulation

2.1 *System Model*

Figure 1 shows a schematic diagram of an MIMO FSO system model with N equal transmitters (an array of partially coherent Gaussian beamlets) and H equal receivers (an array of Gaussian apertures). We assume that beamlets are symmetrically located on the ring with a radius of r_0. Each of the Gaussian beamlets on the ring has a source size of α_s and angle separation of φ_n. At the receiver side, Gaussian apertures with size of R_r are placed on a ring having the radius of r_r with equal angle spacing φ_h. The link distance is L.

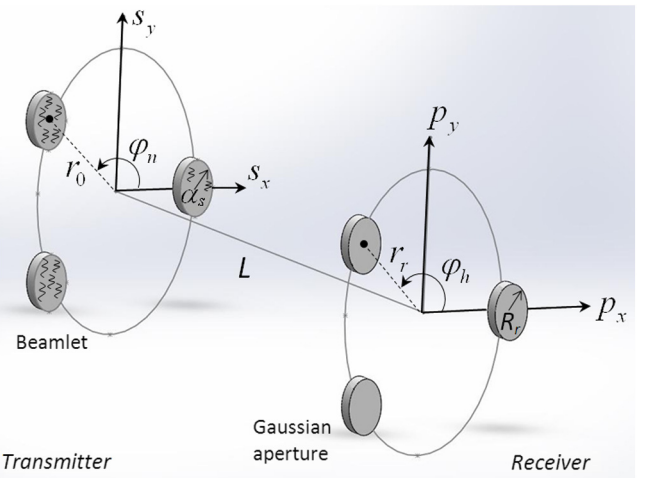

Fig. 1 The schematic diagram of MIMO FSO system with $N = H = 3$.

The total optical field distribution at the transmitter plane for the coherent laser array beam is written as[10]

$$u_c(\mathbf{s}, z=0) = \sum_{n=1}^{N} \exp\{-k\alpha_n[s_x^2 + s_y^2 - 2r_0(s_x \cos\varphi_n + s_y \sin\varphi_n - 0.5r_0)]\}, \quad (1)$$

where $\mathbf{s} = (s_x, s_y)$ is the source transverse coordinate, $\alpha_n = 1/(2k\alpha_s^2)$, $\varphi_n = 2\pi(n-1)/N$, $k = 2\pi/\lambda$ is the wave number, and λ is the wavelength.

Finite-sized receivers, i.e., radial array of Gaussian apertures, can be used to collect the optical intensity and by employing the similar expression used for the laser array at the transmitter plane [10], we have defined here the multi-Gaussian aperture function for the radial array at the receiver plane to be

$$h(\mathbf{p}) = \sum_{h=1}^{H} \exp\left\{-\frac{1}{R_r^2}[p_x^2 + p_y^2 - 2r_r(p_x \cos\varphi_h + p_y \sin\varphi_h) + r_r^2]\right\}, \quad (2)$$

where $\mathbf{p} = (p_x, p_y)$ is the receiver transverse coordinate, $\varphi_h = 2\pi(h-1)/H$. It should be noted that SISO, MISO, SIMO, and MIMO systems can be described, respectively, as ($N = 1$, $r_0 = 0$ and $H = 1$, $r_r = 0$), ($N > 1$, $r_0 > 0$ and $H = 1$, $r_r = 0$), ($N = 1$, $r_0 = 0$ and $H > 1$, $r_r > 0$), and ($N > 1$, $r_0 > 0$ and $H > 1$, $r_r > 0$), respectively.

2.2 *Calculation of the Average Power and the Average of the Square of the Power*

We first calculate the average intensity at the receiver plane, which is then used to calculate the total average power $\langle P \rangle$ and the average of the square of the power $\langle P^2 \rangle$ at the receiver plane. This enables us to calculate the power scintillation index, the receiver-aperture averaging factor and the average BER.

Using the extended Huygens–Fresnel principle, the average intensity at the receiver plane is found to be[1]

$$\langle I(\mathbf{p}, z=L)\rangle = \frac{1}{(\lambda L)^2}\int_{-\infty}^{\infty}\int_{-\infty}^{\infty}\int_{-\infty}^{\infty}\int_{-\infty}^{\infty} \mathbf{ds}_1^2\,\mathbf{ds}_2^2\,\Gamma_2^s(\mathbf{s_1},\mathbf{s_2}) \times \exp\left\{\frac{jk}{2L}\left[(\mathbf{p}-\mathbf{s_1})^2-(\mathbf{p}-\mathbf{s_2})^2\right]-\rho_0^{-2}(\mathbf{s_1}-\mathbf{s_2})^2\right\}, \tag{3}$$

where

$$\Gamma_2^s = \langle u(\mathbf{s}_1, z=0)u^*(\mathbf{s}_2, z=0)\rangle_s, \tag{4}$$

is the source mutual coherence function $j=\sqrt{-1}$, * is the complex conjugate, $\rho_0 = (0.546C_n^2k^2L)^{-3/5}$ is the coherence length of a spherical wave propagating in the turbulent medium, C_n^2 is the structure constant, and $\langle\cdot\rangle_s$ represents the ensemble averaging over the source statistics.

The partially coherent source can be modeled by multiplying the coherent field by the random field[9]

$$u(\mathbf{s}, z=0) = u_c(\mathbf{s}, z=0)u_r(\mathbf{s}, z=0), \tag{5}$$

where $u_r(\mathbf{s}, z=0)$ denotes the random source field through which source partial coherence is introduced. It should be noted that Eq. (5) also implies that the source behaves like a coherent transmission through a diffuser. Employing Eq. (5) into Eq. (4), source mutual coherence function becomes

$$\begin{aligned}\Gamma_2^s &= \langle u(\mathbf{s}_1, z=0)u^*(\mathbf{s}_2, z=0)\rangle_s \\ &= \langle u_c(\mathbf{s_1}, z=0)u_c^*(\mathbf{s_2}, z=0)u_r(\mathbf{s}_1, z=0)u_r^*(\mathbf{s}_2, z=0)\rangle_s \\ &= u_c(\mathbf{s_1}, z=0)u_c(\mathbf{s_2}, z=0)\langle u_r(\mathbf{s}_1, z=0)u_r^*(\mathbf{s}_2, z=0)\rangle_s,\end{aligned} \tag{6}$$

In Eq. (6), the last term $\langle\cdot\rangle_s$ represents the Gaussian mutual coherence function for the source, which is defined as[9]

$$\langle u_r(\mathbf{s}_1, z=0)u_r^*(\mathbf{s}_2, z=0)\rangle_s = \exp\left[-\frac{1}{4\rho_s^2}(\mathbf{s}_1-\mathbf{s}_2)^2\right], \tag{7}$$

where ρ_s is a measure of the degree of source coherence (correlation width of the diffuser) level.[1] Inserting Eqs. (6) and (7) into Eq. (3) and solving Eq. (3) by the repeated use of Eq. 3.323.2 of Ref. 27, we obtain

$$\begin{aligned}\langle I(\mathbf{p}, z=L)\rangle = \pi^2(\lambda L)^{-2}\sum_{n=1}^{N}\sum_{m=1}^{M}\frac{1}{t_1^2t_2^2}\exp(-r_0^2\alpha_s^{-2}) \\ \times\exp\left[-\frac{r_0jk}{2t_1^2\alpha_s^2L}(p_x\cos\varphi_n + p_y\sin\varphi_n)\right. \\ \left.-\frac{k^2}{4t_1^2L^2}(p_x^2+p_y^2)+\frac{r_0^2}{4t_1^2\alpha_s^4}+\frac{1}{4t_2^2}(w_{2x}^2+w_{2y}^2)\right],\end{aligned} \tag{8}$$

where

$$\begin{aligned}t_1^2 &= 0.5\alpha_s^{-2} - 0.5jkL^{-1} + \rho_0^{-2} + 0.25\rho_s^{-2} \\ t_2^2 &= 0.5\alpha_s^{-2} + 0.5jkL^{-1} + \rho_0^{-2} + 0.25\rho_s^{-2} \\ &\quad - t_1^{-2}(\rho_0^{-2}+0.25\rho_s^{-2})^2 \\ w_{2x} &= r_0[\alpha_s^{-2}\cos\varphi_m + t_1^{-2}\alpha_s^{-2}\cos\varphi_n(\rho_0^{-2}+0.25\rho_s^{-2})] \\ &\quad + jkL^{-1}p_x[1-t_1^{-2}(\rho_0^{-2}+0.25\rho_s^{-2})] \\ w_{2y} &= r_0[\alpha_s^{-2}\sin\varphi_m + t_1^{-2}\alpha_s^{-2}\sin\varphi_n(\rho_0^{-2}+0.25\rho_s^{-2})] \\ &\quad + jkL^{-1}p_y[1-t_1^{-2}(\rho_0^{-2}+0.25\rho_s^{-2})].\end{aligned}$$

The average power collected by a finite-sized multi-Gaussian aperture is[1]

$$\langle P\rangle = \int_{-\infty}^{\infty}\int_{-\infty}^{\infty}\langle I(\mathbf{p}, L)\rangle h(\mathbf{p})\mathrm{d}\mathbf{p}. \tag{9}$$

Using Eqs. (2) and (8) into Eq. (9) and performing the integrations over the receiver aperture array, we obtain

$$\begin{aligned}\langle P\rangle &= \frac{\pi^3}{(\lambda L)^2}\frac{1}{t_1^2t_2^2t_p^2}\exp(-r_0^2\alpha_s^{-2}-r_r^2R_r^{-2}) \\ &\times\exp\left(\frac{r_0^2}{4t_1^2\alpha_s^4}\right)\sum_{h=1}^{H}\sum_{n=1}^{N}\sum_{m=1}^{M}\exp\left[\frac{1}{4t_p^2}(w_{px}^2+w_{py}^2)\right] \\ &\times\exp\left\{\frac{r_0^2}{4t_2^2}\left[\cos\varphi_m\frac{1}{\alpha_s^2}+\cos\varphi_n\frac{1}{t_1^2\alpha_s^2}(\rho_0^{-2}+0.25\rho_s^{-2})\right]^2\right\} \\ &\times\exp\left\{\frac{r_0^2}{4t_2^2}\left[\sin\varphi_m\frac{1}{\alpha_s^2}+\sin\varphi_n\frac{1}{t_1^2\alpha_s^2}(\rho_0^{-2}+0.25\rho_s^{-2})\right]^2\right\},\end{aligned} \tag{10}$$

where

$$t_p^2 = \frac{1}{R_r^2}+\frac{k^2}{4t_1^2L^2}+\frac{k^2}{4t_2^2L^2}[1-t_1^{-2}(\rho_0^{-2}+0.25\rho_s^{-2})]^2,$$

$$\begin{aligned}w_{px} &= \frac{jk}{L}\left\{-\frac{r_0\cos\varphi_n}{2t_1^2\alpha_s^2}+\frac{r_0}{2t_2^2}\left[\frac{\cos\varphi_m}{\alpha_s^2}+\frac{\cos\varphi_n}{t_1^2\alpha_s^2}(\rho_0^{-2}+0.25\rho_s^{-2})\right]\right. \\ &\left.\times\left[1-\frac{1}{t_1^2}(\rho_0^{-2}+0.25\rho_s^{-2})\right]\right\}+\frac{2r_r\cos\varphi_h}{R_r^2}, \\ w_{py} &= \frac{jk}{L}\left\{-\frac{r_0\sin\varphi_n}{2t_1^2\alpha_s^2}+\frac{r_0}{2t_2^2}\left[\frac{\sin\varphi_m}{\alpha_s^2}+\frac{\sin\varphi_n}{t_1^2\alpha_s^2}(\rho_0^{-2}+0.25\rho_s^{-2})\right]\right. \\ &\left.\times\left[1-\frac{1}{t_1^2}(\rho_0^{-2}+0.25\rho_s^{-2})\right]\right\}+\frac{2r_r\sin\varphi_h}{R_r^2}.\end{aligned}$$

The average of the square of the power as detected by a finite-sized receiver array having Gaussian apertures function is found to be

$$\langle P^2\rangle = \int_{-\infty}^{\infty}\int_{-\infty}^{\infty}\int_{-\infty}^{\infty}\int_{-\infty}^{\infty}\mathrm{d}^2\mathbf{p}_1d^2\mathbf{p}_2\langle I(\mathbf{p}_1)I(\mathbf{p}_2)\rangle h(\mathbf{p}_1)h(\mathbf{p}_2). \tag{11}$$

The derivation and resulting equation for $\langle P^2\rangle$ are provided in Appendix A.

2.3 *Performance Metrics*

In this section, we define three performance metrics, namely, power scintillation index, aperture averaging factor, and average BER. The power scintillation index (normalized variance of power) quantifies the fluctuations in the received intensity and is defined as[28]

$$m_p^2|_{R_r} = \frac{\langle P^2 \rangle}{\langle P \rangle^2} - 1. \tag{12}$$

The aperture averaging factor is defined as the ratio of power scintillation normalized by the intensity scintillation at the receiver plane origin.[28] Hence

$$G_R = \frac{m_p^2|_{R_r>0}}{m_p^2|_{R_r=0}}, \tag{13}$$

where $m_p^2|_{R_r=0}$ is the intensity scintillation index measured by the point detector at the receiver plane origin. The power scintillation index detected by finite-sized apertures must be lower than a point aperture for effective aperture averaging.

Assuming on–off keying modulation for direct detection receivers, the average BER is calculated as[28]

$$\langle \mathrm{BER} \rangle = \frac{1}{2} \int_0^\infty p_I(i) \operatorname{erfc}\left(i \frac{\langle \mathrm{SNR} \rangle}{2\sqrt{2}} \right) \mathrm{d}i, \tag{14}$$

where $\operatorname{erfc}(\cdot)$ denotes the complementary error function and $\langle \mathrm{SNR} \rangle$ is the average signal-to-noise ratio. In weak turbulence, the intensity I follows the log-normal distribution whose probability density function is given by[1]

$$p_I(I) = \frac{1}{m_p \sqrt{2\pi} I} \exp\left(- \frac{[\ln(I) + 0.5 m_p^2]^2}{2 m_p^2} \right), I > 0, \tag{15}$$

where m_p^2 is defined in Eq. (12) for the MIMO channel. Equation (15) is substituted into Eq. (14) and the resulting expression is numerically evaluated for the $\langle \mathrm{BER} \rangle$ calculation. In Sec. 3, we denote $\langle \mathrm{SNR} \rangle$ and $\langle \mathrm{BER} \rangle$, respectively, as SNR and BER for simplicity.

3 Numerical Results

In this section, numerical results for the power scintillation index, aperture averaging factor, and the average BER are presented based on Eqs. (12), (13), and (14). It should be noted that our results correctly reduce to the partially coherent laser array beam scintillation index in the limiting case for $H = 1$, $r_r = 0$, and $R_r = 0$, i.e., the case without receiver diversity and aperture averaging.[10] Furthermore, we accurately obtain the on-axis scintillation index values of the partially coherent single Gaussian beam by setting $N = 1$, $r_0 = 0$, $H = 1$, $R_r = 0$, and $r_r = 0$ in Ref. 9. For all the figures, we note that the wavelength is chosen as $\lambda = 1.55$ μm and the beamlets are taken to be collimated. The weak turbulence condition (i.e., Rytov variance for the plane wave [1], $1.23 C_n^2 k^{7/6} L^{11/6} < 1$) is satisfied by choosing C_n^2 and L properly.

In Fig. 2, the power scintillation plots of spatial diversity systems such as MISO, SIMO, and MIMO are presented versus the link distance L for different number of beamlets N and receiver apertures H. The power scintillation of a SISO system is also included in Fig. 2 as a benchmark. Specifically, we assume the transmitter ring radius of $r_0 = 2$ cm, source size of $\alpha_s = 1$ cm, receiver ring radius of $r_r = 5$ cm, receiver aperture radius of $R_r = 3$ cm, and the structure constant of atmosphere is $C_n^2 = 1 \times 10^{-15}$ m$^{-2/3}$. We also assume that the beamlets are taken to be coherent source, i.e., the degree of source coherence ($\rho_s \to \infty$). It is observed that the power scintillation increases as the link distance increases. When fixed link distance is considered, as the number of beamlets N and receiver apertures H increase, the power scintillation decreases, and therefore, MIMO system experiences lower scintillation than those in SIMO, MISO, and SISO systems. Furthermore, it is observed that the SIMO system is more effective than the MISO system for the reduction in power scintillation.

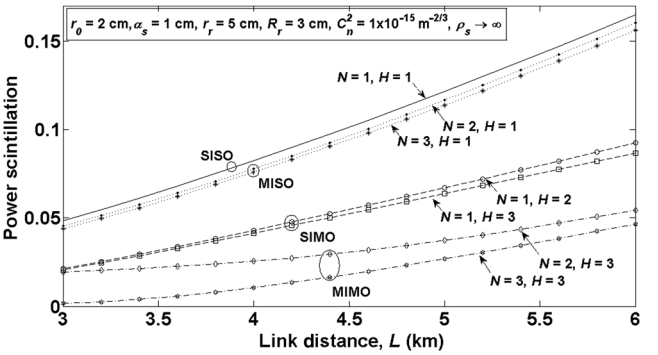

Fig. 2 Power scintillation versus the link distance L for different N and H values.

In Fig. 3, we keep the link distance of $L = 5$ km constant and demonstrate the variation of power scintillation versus receiver aperture radius R_r. The other parameters in Fig. 3 are the same as in Fig. 2. It is observed that the power scintillation decreases as the receiver aperture radius increases. Furthermore, at a fixed R_r, the power scintillation becomes smaller as the number of beamlets N and the number of receiver apertures H increase. The effect of the receiver aperture radius to reduce the power scintillation is more noticeable for SISO and MISO systems. However, the lowest power scintillation is observed for MIMO systems as expected.

In Fig. 4, we consider an SIMO system and investigate the effect of the number of receiver apertures (H) on the power scintillation for different C_n^2 values. Specifically, we assume

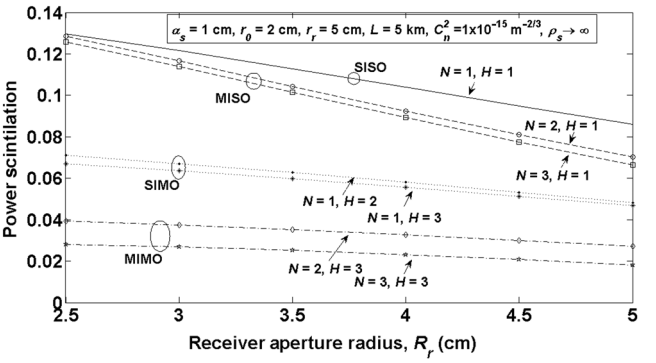

Fig. 3 Power scintillation versus the receiver aperture radius R_r for different N and H values.

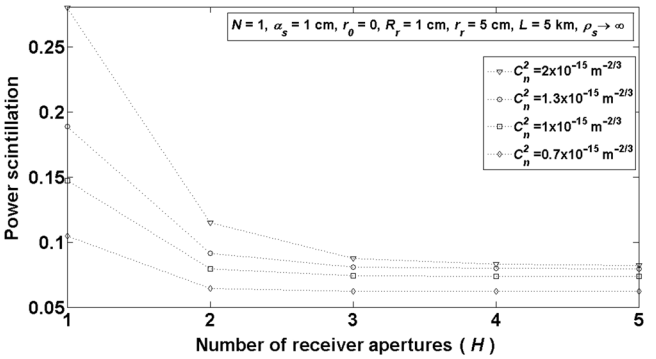

Fig. 4 Power scintillation versus the number of receiver apertures H for different C_n^2 values.

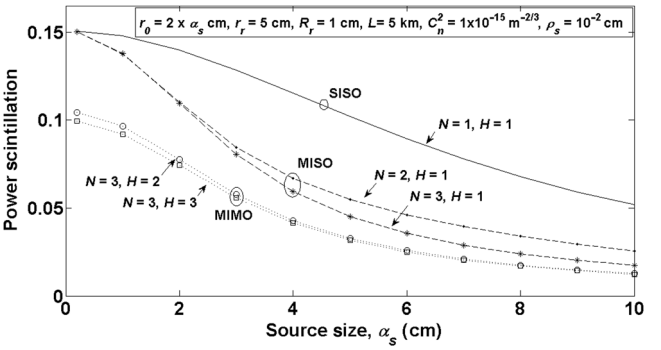

Fig. 6 Power scintillation versus the source size α_s for different N and H values.

a single beamlet $N = 1$ with a source size of $\alpha_s = 1$ cm, transmitter ring radius of $r_0 = 0$, receiver aperture radius $R_r = 1$ cm, receiver ring radius $r_r = 5$ cm, and the link distance $L = 5$ km. Furthermore, the beamlet is assumed to be coherent ($\rho_s \to \infty$). It is observed that increase in the number of receiver apertures (H) up to 3 causes the power scintillation to decrease. However, the power scintillation does not show explicit reductions when > 3 receiver apertures are used. Similar results have been also reported for MISO systems.[23,24] It is also observed that increase in the structure constant C_n^2 causes the power scintillation to increase. The reduction in the power scintillation due to multiple receiver apertures is more pronounced for larger structure constants.

In Fig. 5, the number of receiver apertures $H = 3$ is kept constant and the variation of the power scintillation is illustrated versus the receiver ring radius for various structure constants C_n^2. The other system parameters in Fig. 5 are kept the same as in Fig. 4. It is observed from Fig. 5 that increase in the receiver ring radius causes the power scintillation to decrease. The effect of the receiver ring radius variations on the power scintillation is more noticeable for larger structure constants. This tendency originates from the fact that the field correlation of the received signal becomes smaller for larger structure constants.[22] Thus, receiver apertures experience statistically independent channel when the ring radius is increased and therefore decrease in the power scintillation is observed.

In Fig. 6, we assume an array of partially coherent source at the transmitter and investigate the variation of the source size α_s on the power scintillation for different number of beamlets N and receiver apertures H. Specifically, the transmitter ring radius is arranged as $r_0 = 2\alpha_s$ to avoid overlapping of the beamlet fields and the degree of source coherence is also set as $\rho_s = 10^{-2}$ cm to obtain partially coherent source. The other system parameters are fixed. It is observed that the power scintillation decreases as the source size increases. At a fixed source size, increase in N and H causes the power scintillation to decrease.

Figure 7 shows the variation of the aperture averaging factor of diversity systems against the receiver aperture radius R_r for different number of beamlets N and receiver apertures H, keeping the other system parameters fixed. The observation from Fig. 7 is that the aperture averaging factor decreases as the receiver aperture radius increases. At a fixed size of R_r, the lowest averaging factor is observed for the largest number of beamlets and the largest number of receiver apertures. Thus, as N and H increase, the aperture averaging factor decreases. The change in the aperture averaging factor for SIMO and MIMO systems is relatively small with respect to SISO and MISO systems.

In Figs. 8–11, we investigate the effect of several system parameters on the BER based on Eq. (14) and the power scintillation index values obtained from Figs. 2–6. In these figures, we assume that the structure constant of the atmosphere and link distance are chosen as $C_n^2 = 1 \times 10^{-15}$ m$^{-2/3}$ and $L = 5$ km, respectively. As a benchmark, the BER for SISO system is also provided.

In Fig. 8, we illustrate the effect of the number of transmitter beamlets N and receiver apertures H on the BER. We assume transmitter ring radius of $r_0 = 2$ cm, source size of

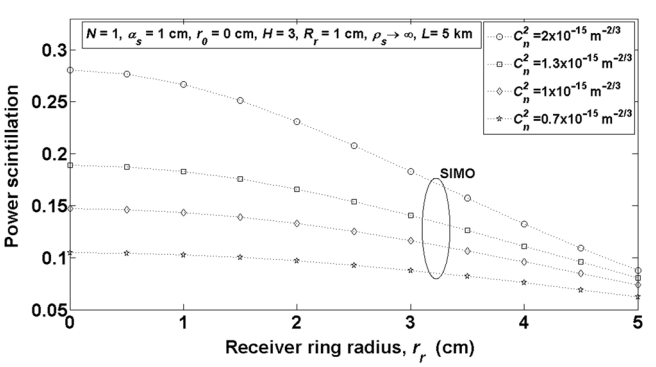

Fig. 5 Power scintillation versus the receiver ring radius r_r for different C_n^2 values.

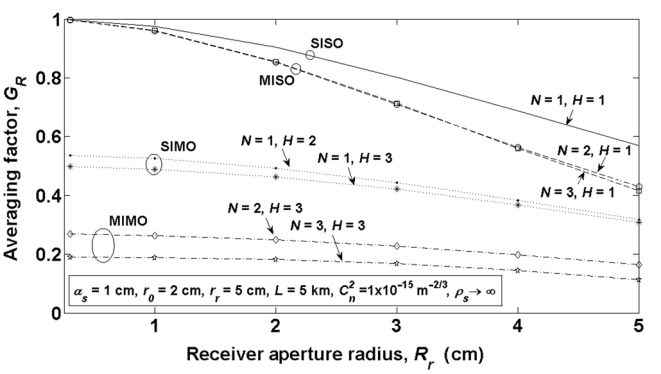

Fig. 7 Receiver aperture averaging factor G_R versus the receiver aperture radius R_r for different N and H values.

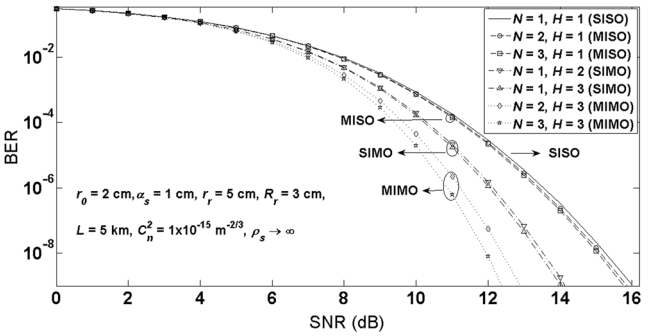

Fig. 8 BER versus SNR for different N and H values.

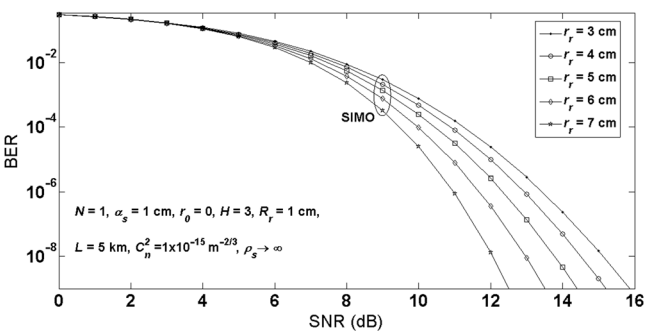

Fig. 9 BER versus SNR for different r_r values.

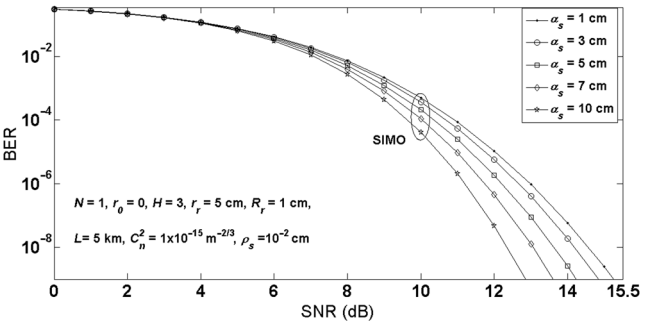

Fig. 10 BER versus SNR for different α_s values.

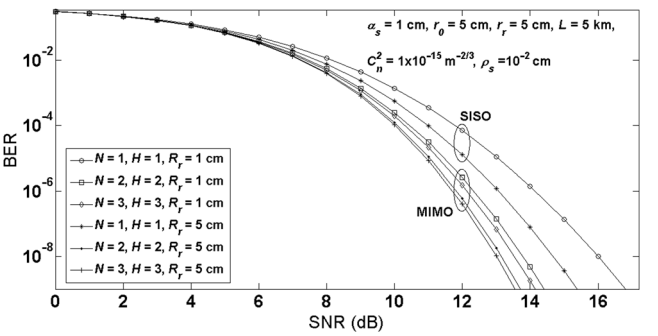

Fig. 11 BER versus SNR for $N = H = 1,2$, and 3 values.

$\alpha_s = 1$ cm, receiver ring radius $r_r = 5$ cm and receiver aperture radius $R_r = 3$ cm. Furthermore, the beamlets are assumed to be coherent source ($\rho_s \to \infty$;). It is observed that BER decreases as N and H increase. At a fixed SNR, SIMO systems are more effective than MISO systems for BER improvement. The lowest BER is observed for the MIMO system as expected. For example, to achieve a targeted BER of 10^{-9}, an SNR of 16 dB is required for the SISO system. This reduces to (15.8, 15.7), (14.2, 14.1), and (12.8, 12.4) dB, respectively, for MISO ($N = 2$ and 3), SIMO ($H = 2$ and 3), and MIMO ($N = 2$, $H = 3$, and $N = 3$, $H = 3$) systems.

In Fig. 9, we consider an SIMO FSO system with receiver aperture radius of $R_r = 1$ cm, number of receiver apertures of $H = 3$, and the source size of $\alpha_s = 1$ cm. We examine the effect of the receiver ring radius r_r on the BER. At a fixed SNR, increase in the receiver ring radius causes the BER to decrease. For example, to achieve a targeted BER of 10^{-9}, SNRs of 15.8, 15.2, 14.4, 13.5, and 12.5 dB are required, respectively, for $r_r = 3$,4,5,6, and 7 cm. Improvements in the BER is small due to weak atmospheric turbulence.

In Fig. 10, we keep the receiver ring radius of $r_r = 5$ cm and the number of receiver apertures $H = 3$ constant and investigate the impact of the source size α_s on the BER for a partially coherent source ($\rho_s = 10^{-2}$ cm). At a fixed SNR, BER decreases as the source size increases. For example, to achieve a targeted BER of 10^{-9}, SNRs of 15.2, 14.8, 14.2, 13.6, and 12.8 dB are required, respectively, for $\alpha_s = 1$,3,5,7, and 10 cm.

Finally, we investigate the effect of the receiver aperture radius R_r on the BER for SISO and MIMO systems. In Fig. 11, the number of beamlets N and receiver apertures H are chosen as $N = H = 1$,2, and 3, while the R_r is set as 1 and 5 cm. We assume partially coherent beamlets with size of $\alpha_s = 1$ cm. The transmitter and receiver ring radius are set as 5 cm. At a fixed SNR, increase in the receiver aperture radius causes the BER to decrease prominently. BER also decreases as the N and H increase. The effect of R_r to reduce the BER is more apparent in the SISO system. To achieve a targeted BER of 10^{-9}, SNR of 16.8, and 15.3 dB are required, respectively, for ($N = H = 1$, $R_r = 1$ cm and ($N = H = 1$, $R_r = 5$ cm). This reduces to 14.4 and 14.1 dB, respectively, for ($N = H = 2$, $R_r = 1$ cm) and ($N = H = 3$, $R_r = 1$ cm). This further reduces to 13.7, 13.6 dB, respectively, for ($N = H = 2$, $R_r = 5$ cm) and ($N = H = 3$, $R_r = 5$ cm). It is noticed that aperture averaging has a strong effect on the BER.

4 Conclusion

In this paper, a comprehensive performance analysis of MIMO FSO systems with Gaussian beams and finite-sized detectors is performed. Various performance metrics such as power scintillation index, the aperture averaging factor, and the average BER are scrutinized by examining the system parameters. Both coherent and partially coherent laser beams are considered. For the coherent beams, it is found that the power scintillation and the aperture averaging factor decrease as the number of transmitter beamlets, receiver apertures, and the receiver aperture radius increase. The reduction in the power scintillation due to multiple receiver apertures is more pronounced for larger structure constants. It is also found that the power scintillation does not show much variation when the number of receiver apertures are chosen beyond 3. Furthermore, an increase in the receiver ring radius causes the power scintillation to decrease. The effect of the receiver ring radius variations on the power

scintillation is more noticeable for larger structure constants. Similarly, BER decreases as the receiver ring radius, the number of transmitter beamlets, and receiver apertures increase. For partially coherent beams, it is found that the power scintillation decreases as the number of transmitter beamlets and receiver apertures increase. Furthermore, a larger source size makes the power scintillation decrease. The ability of source size for scintillation reduction is more apparent for MISO systems than those in SISO and MIMO systems. Similarly, BER decreases as the source size, the number of transmitter beamlets and receiver apertures increase. In all the figures, we have found that the MIMO system shows better performance than those in SISO, MISO, and SIMO systems.

Appendix

This appendix shows the calculation of $\langle P^2\rangle$. First, we need to calculate $\langle I(\mathbf{p_1})I(\mathbf{p}_2)\rangle$, given by[4]

$$\langle I(\mathbf{p_1})I(\mathbf{p_2})\rangle = \frac{1}{(\lambda L)^4}\int_{-\infty}^{\infty}\int_{-\infty}^{\infty}\mathrm{d}^2\mathbf{s}_1\int_{-\infty}^{\infty}\int_{-\infty}^{\infty}\mathrm{d}^2\mathbf{s}_2 \times\int_{-\infty}^{\infty}\int_{-\infty}^{\infty}\mathrm{d}^2\mathbf{s}_3\int_{-\infty}^{\infty}\int_{-\infty}^{\infty}\mathrm{d}^2\mathbf{s}_4\langle u(\mathbf{s}_1)u^*(\mathbf{s_2})\rangle_s\langle u(\mathbf{s}_3)u^*(\mathbf{s_4})\rangle_s \times\exp\left[\frac{jk}{2\,L}(|\mathbf{p_1}-\mathbf{s_1}|^2-|\mathbf{p_1}-\mathbf{s_2}|^2+|\mathbf{p_2}-\mathbf{s_3}|^2-|\mathbf{p_2}-\mathbf{s_4}|^2)\right] \times\langle\exp[\psi(\mathbf{s}_1,\mathbf{p_1})+\psi^*(\mathbf{s}_2,\mathbf{p_1})+\psi(\mathbf{s}_3,\mathbf{p_2})+\psi^*(\mathbf{s}_4,\mathbf{p_2})]\rangle_m. \tag{16}$$

The second line of Eq. (16) is the fourth-order source coherence function for detection time larger than the source coherence time (i.e., slow detector). The last line of Eq. (16) is the fourth-order spherical-wave coherence function of the medium, $\langle\cdot\rangle_m$ denotes the ensemble average over the statistics of turbulent medium. In weak turbulence, log-amplitude and phase fluctuations are assumed to have Gaussian statistics which yield[4]

$$\begin{aligned}\langle\exp[\psi(\mathbf{s}_1,\mathbf{p_1})+\psi*(\mathbf{s}_2,\mathbf{p_1})+\psi(\mathbf{s}_3,\mathbf{p_2})+\psi*(\mathbf{s}_4,\mathbf{p_2})]\rangle_m &= [1+2B_\chi(\mathbf{s}_1-\mathbf{s}_3,\mathbf{p}_d)+2B_\chi(\mathbf{s}_2-\mathbf{s}_4,\mathbf{p}_d)]\\ &\times\exp[-0.5D_\psi(\mathbf{s}_1-\mathbf{s}_2,0)-0.5D_\psi(\mathbf{s}_3-\mathbf{s}_4,0)\\ &-0.5D_\psi(\mathbf{s}_2-\mathbf{s}_3,\mathbf{p}_d)-0.5D_\psi(\mathbf{s}_1-\mathbf{s}_4,\mathbf{p}_d)\\ &+0.5D_\psi(\mathbf{s}_1-\mathbf{s}_3,\mathbf{p}_d)+0.5D_\psi(\mathbf{s}_2-\mathbf{s}_4,\mathbf{p}_d)\\ &+jD_{\chi S}(\mathbf{s}_2-\mathbf{s}_4,\mathbf{p}_d)-jD_{\chi S}(\mathbf{s}_1-\mathbf{s}_3,\mathbf{p}_d)],\end{aligned} \tag{17}$$

where $B_\chi(\mathbf{s}_r-\mathbf{s}_q,\mathbf{p}_d)=\sigma_{\chi_s}^2\exp[-\frac{1}{\rho_0^2}(|\mathbf{s}_r-\mathbf{s}_q|^2+|\mathbf{s}_r-\mathbf{s}_q|\cdot\mathbf{p}_d+\mathbf{p}_d^2)]$, with $r=1,2$ and $q=3,4$ is the log-amplitude correlation function, $\sigma_{\chi_s}^2=0.124\ k^{7/6}C_n^2L^{11/6}$ is the spherical wave log-amplitude variance. $B_x\ll 1$ is taken for approximation in weak turbulence[7] and $D_\psi(\mathbf{s}_d,\mathbf{p}_d)=2\rho_0^{-2}(\mathbf{s}_d^2+\mathbf{s}_d.\mathbf{p}_d+\mathbf{p}_d^2)$ is the wave structure function under quadratic approximation.[29] The validation of the wave structure function[4] is within $l_0\ll|\mathbf{s_d}|\ll\sqrt{\lambda L}$. Here, l_0 is the inner scale of turbulence, $|\mathbf{s}_d|$ is the difference of the transverse source coordinates, and $\sqrt{\lambda L}$ is the Fresnel zone. $D_{\chi S}(\mathbf{s}_d,\mathbf{p}_d)=\rho_{\chi S}^{-2}(\mathbf{s}_d^2+\mathbf{s}_d.\mathbf{p}_d+\mathbf{p}_d^2)$ is the log-amplitude phase structure function, $\rho_{\chi S}=(0.114C_n^2k^{13/6}L^{5/6})^{-1/2}$ is the coherence length of log-amplitude and phase. Inserting Eqs. (6) and (17) into Eq. (16), using the resulting expression in Eq. (11), the equation for $\langle P^2\rangle$ is found to be

$$\langle P^2\rangle=\sum_{i=1}^{3}Z_i, \tag{18}$$

where

$$\begin{aligned}Z_i = E_i(\lambda L)^{-4}\pi^6\exp(-2r_r^2R_r^{-2})&\sum_{h=1}^{H}\sum_{f=1}^{H}\sum_{n=1}^{N}\sum_{m=1}^{N}\sum_{l=1}^{N}\sum_{o=1}^{N}\\ &\times\exp[-r_0^2k(\alpha_n+\alpha_m+\alpha_l+\alpha_o)]\\ &\times\exp\left(\frac{\cos^2\varphi_nk^2\alpha_n^2r_0^2}{\beta_1^2}+\frac{F_{1x}^2}{4\beta_2^2}+\frac{F_{6x}^2}{4\beta_3^2}+\frac{F_{10x}^2}{4\beta_4^2}+\frac{F_{13x}^2}{4\beta_{1p}^2}\right)\\ &\times\exp\left(\frac{\sin^2\varphi_nk^2\alpha_n^2r_0^2}{\beta_1^2}+\frac{F_{1y}^2}{4\beta_2^2}+\frac{F_{6y}^2}{4\beta_3^2}+\frac{F_{10y}^2}{4\beta_4^2}+\frac{F_{13y}^2}{4\beta_{1p}^2}\right)\\ &\times\exp[0.25\beta_{2p}^{-2}(q_{2px}^2+q_{2py}^2)](\beta_1\beta_2\beta_3\beta_4\beta_{1p}\beta_{2p})^{-2},\end{aligned} \tag{19}$$

$$F_{1x}=\frac{2\cos\varphi_nk\alpha_nr_0}{\beta_1^2\rho_0^2}+k\alpha_m2r_0\cos\varphi_m+\frac{\cos\varphi_nk\alpha_nr_0}{2\beta_1^2\rho_s^2},$$

$$F_2=(-jkL^{-1}-\rho_0^{-2}+T)\left(\frac{1}{\beta_1^2\rho_0^2}+\frac{1}{4\beta_1^2\rho_s^2}\right)+\frac{jk}{L}-\frac{1}{\rho_0^2}+R,$$

$$F_3=\left(\frac{1}{\rho_0^2}-T\right)\left(\frac{1}{\beta_1^2\rho_0^2}+\frac{1}{4\beta_1^2\rho_s^2}\right)+\frac{1}{\rho_0^2}-R,$$

$$F_4=\frac{2}{\rho_0^2}-\frac{2T}{\beta_1^2\rho_0^2}-\frac{T}{2\rho_s^2\beta_1^2},$$

$$F_5=\frac{2}{\beta_1^2\rho_0^4}+\frac{1}{2\beta_1^2\rho_0^2\rho_s^2}-2R$$

$$F_{6x}=\frac{F_{1x}F_4}{2\beta_2^2}-\frac{\cos\varphi_nk\alpha_nr_02T}{\beta_1^2}+\cos\varphi_lk\alpha_l2r_0,$$

$$F_7=\frac{F_2F_4}{2\beta_2^2}-\frac{1}{\beta_1^2}(-jkL^{-1}-\rho_0^{-2}+T)T+\frac{1}{\rho_0^2}-T,$$

$$F_8=\frac{F_3F_4}{2\beta_2^2}-\frac{T}{\beta_1^2}\left(\frac{1}{\rho_0^2}-T\right)-\frac{jk}{L}-\frac{1}{\rho_0^2}+T,$$

$$F_9=\frac{F_4F_5}{2\beta_2^2}-\frac{2T}{\beta_1^2\rho_0^2}+2\left(\frac{1}{\rho_0^2}+\frac{1}{4\rho_s^2}\right),$$

$$F_{10x}=\frac{F_{6x}F_9}{2\beta_3^2}+\frac{F_{1x}F_5}{2\beta_2^2}+\cos\varphi_nk\alpha_nr_0\frac{2}{\beta_1^2\rho_0^2}+\cos\varphi_ok\alpha_o2r_0,$$

$$F_{11}=\frac{F_7F_9}{2\beta_3^2}+\frac{F_2F_5}{2\beta_2^2}+(-jkL^{-1}-\rho_0^{-2}+T)\frac{1}{\beta_1^2\rho_0^2}+\frac{1}{\rho_0^2}-R,$$

$$F_{12}=\frac{F_8F_9}{2\beta_3^2}+\frac{F_3F_5}{2\beta_2^2}+\frac{1}{\beta_1^2\rho_0^2}\left(\frac{1}{\rho_0^2}-T\right)+\frac{jk}{L}-\frac{1}{\rho_0^2}+R,$$

$$F_{13x}=\frac{2r_r}{R_r^2}\cos\varphi_h+\frac{\cos\varphi_n k\alpha_n r_0}{\beta_1^2}(-jkL^{-1}-\rho_0^{-2}+T)+\frac{F_{1x}F_2}{2\beta_2^2}+\frac{F_{6x}F_7}{2\beta_3^2}+\frac{F_{10x}F_{11}}{2\beta_4^2},$$

$$F_{14}=\frac{1}{2\beta_1^2}(-jkL^{-1}-\rho_0^{-2}+T)\left(\frac{1}{\rho_0^2}-T\right)+\frac{F_2F_3}{2\beta_2^2}+\frac{F_7F_8}{2\beta_3^2}+\frac{F_{11}F_{12}}{2\beta_4^2}+\frac{4}{\rho_0^2}-2(T+R),$$

$$\beta_{1p}^2=\frac{1}{R_r^2}-\frac{1}{4\beta_1^2}(-jkL^{-1}-\rho_0^{-2}+T)^2-\frac{F_2^2}{4\beta_2^2}-\frac{F_7^2}{4\beta_3^2}-\frac{F_{11}^2}{4\beta_4^2}+\frac{2}{\rho_0^2}-(T+R),$$

$$\beta_{2p}^2=\frac{1}{R_r^2}-\frac{F_{14}^2}{4\beta_{1p}^2}-\frac{1}{4\beta_1^2}\left(\frac{1}{\rho_0^2}-T\right)^2-\frac{F_3^2}{4\beta_2^2}-\frac{F_8^2}{4\beta_3^2}-\frac{F_{12}^2}{4\beta_4^2}+\frac{2}{\rho_0^2}-(T+R),$$

$$\beta_2^2=-\frac{1}{\beta_1^2\rho_0^4}-\frac{1}{16\beta_1^2\rho_s^4}-\frac{1}{\beta_1^2\rho_0^2 2\rho_s^2}+\theta_1^2,$$

$$\beta_3^2=-\frac{F_4^2}{4\beta_2^2}-\frac{T^2}{\beta_1^2}+\varsigma_1^2,$$

$$\beta_4^2=-\frac{F_9^2}{4\beta_3^2}-\frac{F_5^2}{4\beta_2^2}-\frac{1}{\beta_1^2\rho_0^4}+\xi_1^2,$$

$$\beta_1^2=k\alpha_n-0.5jkL^{-1}+2\rho_0^{-2}-T+0.25\rho_s^{-2}$$
$$\theta_1^2=k\alpha_m+0.5jkL^{-1}-R+2\rho_0^{-2}+0.25\rho_s^{-2},$$
$$\varsigma_1^2=k\alpha_l-0.5jkL^{-1}+2\rho_0^{-2}-T+0.25\rho_s^{-2},$$
$$\xi_1^2=k\alpha_o+0.5jkL^{-1}-R+2\rho_0^{-2}+0.25\rho_s^{-2},$$

$$q_{2px}=\frac{2r_r}{R_r^2}\cos\varphi_f+\frac{F_{13x}F_{14}}{2\beta_{1p}^2}+\frac{\cos\varphi_n k\alpha_n r_0}{\beta_1^2}\left(\frac{1}{\rho_0^2}-T\right)+\frac{F_{1x}F_3}{2\beta_2^2}+\frac{F_{6x}F_8}{2\beta_3^2}+\frac{F_{10x}F_{12}}{2\beta_4^2},$$

$$\text{In } Z_1;E_1=1,T=-\frac{j}{\rho_{\chi S}^2}+\frac{1}{\rho_0^2},R=\frac{j}{\rho_{\chi S}^2}+\frac{1}{\rho_0^2},$$

$$\text{In } Z_2;E_2=2\sigma_{\chi_S}^2,T=-\frac{j}{\rho_{\chi S}^2},R=\frac{j}{\rho_{\chi S}^2}+\frac{1}{\rho_0^2},$$

$$\text{In } Z_3;E_3=2\sigma_{\chi_S}^2,T=-\frac{j}{\rho_{\chi S}^2}+\frac{1}{\rho_0^2},R=\frac{j}{\rho_{\chi S}^2}.$$

Here, F_{1y}, F_{6y}, F_{10y}, F_{13y}, q_{2py} are obtained by, respectively, replacing all the cosine functions in F_{1x}, F_{6x}, F_{10x}, F_{13x}, q_{2px} by the sine functions.

Acknowledgments

M.C. Gökçe, Y. Baykal, and M. Uysal acknowledge the support provided by Çankaya University and Özyeğin University, respectively. M.C. Gökçe gratefully acknowledges the financial support from TÜBİTAK 2211-C. The work of M. Uysal is carried out as an activity of the Centre of Excellence in Optical Wireless Communication Technologies (OKATEM), funded by the Istanbul Development Agency (ISTKA) under the Innovative Istanbul Financial Support Program, 2015. The statements made herein are solely the responsibility of the authors and do not reflect the views of ISTKA or T.R. Ministry of Development.

References

1. L. C. Andrews and R. L. Philips, *Laser Beam Propagation Through Random Media*, SPIE Press, Bellingham, Washington (2005).
2. V. I. Tatarskii, *The Effects of the Turbulent Atmosphere on Wave Propagation*, National Technical Information Service, Springfield (1971).
3. L. C. Andrews, "Aperture-averaging factor for optical scintillations of plane and spherical waves in the atmosphere," *J. Opt. Soc. Am. A* **9**(4), 597–600 (1992).
4. S. J. Wang, Y. Baykal, and M. A. Plonus, "Receiver-aperture averaging effects for the intensity fluctuation of a beam wave in the turbulent atmosphere," *J. Opt. Soc. Am.* **73**(6), 831–837 (1983).
5. C. Kamacıoğlu, Y. Baykal, and E. Yazgan, "Averaging of receiver aperture for flat-topped incidence," *Opt. Laser Technol.* **52**, 91–95 (2013).
6. C. Kamacıoğlu, Y. Baykal, and E. Yazgan, "Receiver-aperture averaging of annular beams propagating through turbulent atmosphere," *Opt. Eng.* **52**(12), 126103 (2013).
7. R. L. Fante, "Intensity fluctuations of an optical wave in a turbulent medium effect of source coherence," *Opt. Acta Int. J. Opt.* **28**(9), 1203–1207 (1981).
8. Y. Baykal, M. A. Plonus, and S. J. Wang, "The scintillations for weak atmospheric turbulence using a partially coherent source," *Radio Sci.* **18**(4), 551–556 (1983).
9. Y. Baykal, H. T. Eyyuboğlu, and Y. Cai, "Scintillations of partially coherent multiple Gaussian beams in turbulence," *Appl. Opt.* **48**(10), 1943–1954 (2009).
10. Ç. Arpali et al., "Intensity fluctuations of partially coherent laser beam arrays in weak atmospheric turbulence," *Appl. Phys. B* **103**(1), 237–244 (2011).
11. I. E. Lee et al., "Effects of aperture averaging and beam width on a partially coherent Gaussian beam over free-space optical links with turbulence and pointing errors," *Appl. Opt.* **55**(1), 1–9 (2016).
12. A. Efimov, K. Velizhanin, and G. Gelikonov, "Simultaneous scintillation measurements of coherent and partially coherent beams in an open atmosphere experiment," *Proc. SPIE* **8971**, 897105 (2014).
13. A. A. Farid and S. Hranilovic, "Outage capacity for MISO intensity-modulated free space optical links with misalignment," *J. Opt. Commun. Netw.* **3**(10), 780–789 (2011).
14. M. Safari and S. Hranilovic, "Diversity gain for near-field MISO atmospheric optical communications," in *Proc. IEEE Conf. on Communication*, pp. 3128–3132 (2012).
15. M. A. Khalighi et al., "Fading reduction by aperture averaging and spatial diversity in optical wireless systems," *J. Opt. Commun. Netw.* **1**(6), 580–593 (2009).
16. S. M. Navidpour, M. Uysal, and M. Kavehrad, "BER performance of free-space optical transmission with spatial diversity," *IEEE Trans. Wireless Commun.* **6**(8), 2813–2819 (2007).
17. E. J. Lee and V. W. S. Chan, "Part 1: Optical communication over the clear turbulent atmospheric channel using diversity," *IEEE J. Sel. Areas Commun.* **22**(9), 1896–1906 (2004).

18. J. A. Anguita, M. A. Neifeld, and B. V. Vasic, "Spatial correlation and irradiance statistics in a multiple-beam terrestrial free-space optical communication link," *Appl. Opt.* **46**(26), 6561–6571 (2007).
19. N. Letzepis and A. G. I. Fabregas, "Outage probability of the Gaussian MIMO free-space optical channel with PPM," *IEEE Trans. Commun.* **57**(12), 3682–3690 (2009).
20. P. Kaur, V. K. Jain, and S. Kar, "Performance analysis of free space optical links using multi-input multi-output and aperture averaging in presence of turbulence and various weather conditions," *IET Commun.* **9**(8), 1104–1109 (2015).
21. I. I. Kim et al., "Scintillation reduction using multiple transmitters," *Proc. SPIE* **2990**, 102–113 (1997).
22. Y. Baykal, "Field correlation of laser arrays in atmospheric turbulence," *Appl. Opt.* **53**(7), 1284–1289 (2014).
23. M. C. Gökçe et al., "Aperture averaging in multiple-input single-output free-space optical systems," *Opt. Eng.* **54**(6), 066103 (2015).
24. M. C. Gökçe et al., "Performance analysis of MIMO FSO systems with radial array beams and finite sized detectors," *Proc. SPIE* **9224**, 922409 (2014).
25. M. C. Gökçe, Y. Baykal, and M. Uysal, "Aperture averaging in multiple-input single-output free-space optical systems using partially coherent radial array beams," *J. Opt. Soc. Am. A* **33**(6), 1041–1048 (2016).
26. M. C. Gökçe, Y. Baykal, and M. Uysal, "Bit error rate analysis of MISO FSO systems," *Wave Random Complex Media* **26**(4), 642–649 (2016).
27. I. S. Gradshteyn and I. M. Ryzhik, *Tables of Integrals, Series and Products*, Academic Press Inc., New York (2000).
28. L. C. Andrews, R. L. Philips, and C. Y. Hopen, *Laser Beam Scintillation with Applications*, SPIE Press, Bellingham, Washington (2001).
29. J. C. Leader, "Atmospheric propagation of partially coherent radiation," *J. Opt. Soc. Am.* **68**(2), 175–185 (1978).

Muhsin Caner Gökçe received his BSc degree in electronic and communication engineering from Çankaya University, Ankara, Turkey, in 2009, and his MS degree in electrical and electronics engineering from Ankara University, Ankara, Turkey, in 2012. He is currently working toward a PhD in electronic and communication engineering at Çankaya University. His current research interest is multiple-input multiple-output free-space optical communications. He is working as a specialist at Çankaya University.

Yahya Baykal received his PhD from Northwestern University, Evanston, Illinois, USA, in 1982. He worked as a manager in R&D of Teletaş (Alcatel), Türk Philips Trades A.Ş., and as the general manager at İltek Telekomünikasyon (Iskratel) Company. He is currently the chairman of Electrical-Electronics Engineering Department, Çankaya University, Ankara, Turkey. He lectures in the areas of telecommunication networks. His main research areas cover atmospheric and underwater optical wireless systems. He is the author of 124 SCI and 60 conference papers.

Murat Uysal received his BSc and MSc degrees in electronics and communication engineering from İstanbul Technical University, İstanbul, Turkey, in 1995 and 1998, respectively, and his PhD in electrical engineering from Texas A&M University, College Station, Texas, USA, in 2001. He is currently a full professor and chair of the Department of Electrical and Electronics Engineering at Özyeğin University, İstanbul, Turkey.